ADVANCED MATERIALS
www.advmat.de

Interfacial Defect Vibrations Enhance Thermal Transport in Amorphous Multilayers with Ultrahigh Thermal Boundary Conductance

Ashutosh Giri, Sean W. King, William A. Lanford, Antonio B. Mei, Devin Merrill, Liyi Li, Ron Oviedo, John Richards, David H. Olson, Jeffrey L. Braun, John T. Gaskins, Freddy Deangelis, Asegun Henry, and Patrick E. Hopkins**

The role of interfacial nonidealities and disorder on thermal transport across interfaces is traditionally assumed to add resistance to heat transfer, decreasing the thermal boundary conductance (TBC). However, recent computational studies have suggested that interfacial defects can enhance this thermal boundary conductance through the emergence of unique vibrational modes intrinsic to the material interface and defect atoms, a finding that contradicts traditional theory and conventional understanding. By manipulating the local heat flux of atomic vibrations that comprise these interfacial modes, in principle, the TBC can be increased. In this work, experimental evidence is provided that interfacial defects can enhance the TBC across interfaces through the emergence of unique high-frequency vibrational modes that arise from atomic mass defects at the interface with relatively small masses. Ultrahigh TBC is demonstrated at amorphous SiOC:H/SiC:H interfaces, approaching 1 GW m^{-2} K^{-1} and are further increased through the introduction of nitrogen defects. The fact that disordered interfaces can exhibit such high conductances, which can be further increased with additional defects, offers a unique direction to manipulate heat transfer across materials with high densities of interfaces by controlling and enhancing interfacial thermal transport.

Heterogeneous interfaces between two adjacent solids have enabled the realization of ultralow thermal conductivity materials,[1–5] with reduction to thermal conductivity often falling below the corresponding minimum limit traditionally attributed to a pure amorphous solid.[6] These reductions in thermal conductivity have been driven by additional temperature drops occurring at each interface. These temperature drops are quantified by the thermal boundary conductance (TBC), which is traditionally assumed to be related to the phonon states in each material comprising the interface. While lowering effective thermal conductivity by adding interfaces is great for thermoelectric and thermal barrier coating applications, it is highly undesirable for microelectronic applications where there is a need to dissipate ever increasing amounts of waste heat thanks to continued miniaturization leading to increased device and interface density. More specifically, increased interface density may be good for thermal insulation applications but is bad from a thermal perspective for microelectronic devices. Thus, the approach of engineering materials with high densities of interfaces to achieve ultralow thermal conductivity solids requires a fundamental understanding of how atomic vibrations interact and exchange energy at interfaces, which, with the advent of disorder and other nanoscale features, is arguably lacking.

While including disorder in a crystalline system can lead to reductions in thermal conductivity, this same phenomena may not hold true at interfaces. Recent theories have suggested that

Dr. A. Giri, D. H. Olson, J. L. Braun, Dr. J. T. Gaskins, Prof. P. E. Hopkins
Department of Mechanical and Aerospace Engineering
University of Virginia
Charlottesville, VA 22904, USA
E-mail: ag4ar@virginia.edu; peh4v@virginia.edu

Dr. S. W. King, Dr. A. B. Mei, Dr. D. Merrill, Dr. L. Li, R. Oviedo, J. Richards
Intel Corporation
Logic Technology Development
5200 NE Elam Young Parkway, Hillsboro, OR 97124, USA

The ORCID identification number(s) for the author(s) of this article can be found under https://doi.org/10.1002/adma.201804097.

Prof. W. A. Lanford
Department of Physics
University at Albany
State University of New York
Albany, NY 12222, USA

F. Deangelis, Prof. A. Henry
The George W. Woodruff School of Mechanical Engineering
Georgia Institute of Technology
Atlanta, GA 30332, USA

Prof. A Henry
Department of Mechanical Engineering
Massachusetts Institute of Technology
Cambridge, 02139 Massachusetts, USA

DOI: 10.1002/adma.201804097

vibrational modes unique to the interfaces that do not exist intrinsically in any of the homogeneous materials can in fact contribute substantially to the TBC.[7–11] Therefore, judiciously selected defects near the interface could in principle be used to increase the TBC by enhancing these interfacial modes. In this case, disordered interfaces could lead to higher TBCs than more "perfect" interfaces. Indeed, recent computational works have demonstrated that the TBC at amorphous/amorphous and amorphous/crystalline interfaces can be higher than that at crystalline/crystalline interfaces composed of the same material.[12,13] This reasoning cannot be explained by conventional phonon TBC theories[14–16] and offers a unique picture of how vibrational energy couples across defected or disordered interfaces. However, experimental demonstrations of the existence of these interfacial defect modes and their contributions to TBC are lacking.

In this work, we report on the thermal conductivity of a series of amorphous multilayers (AMLs) composed of alternating layers of hydrogenated amorphous silicon carbide (a-SiC:H) and hydrogenated amorphous silicon oxycarbide (a-SiOC:H) with varying interface densities. One of the main reasons for studying these material systems stems from a practicality standpoint, as the existence of these particular amorphous systems is widespread in high density, highly integrated microelectronic products mainly due to their low dielectric constants.[17] This is particularly the case in metal interconnect structures where multiple layers of amorphous dielectric materials are stacked upon one another and inlaid with Cu lines. In this regard, the SiC:H/SiOC:H system investigated is highly relevant as SiC:H represents the Cu capping/etch stop layer and the SiOC:H material represents the interlayer dielectric material that isolates the Cu lines.

As the heat transport in these AMLs is completely diffusive, we extract a TBC across the a-SiC:H/a-SiOC:H interface that approaches 1 GW m^{-2} K^{-1}, the highest diffusive TBC measured to date. Through an in situ plasma exposure, we introduce N_2 defects at and near the interface in each layer of the AML. The introduction of these defects causes the thermal conductivity of these AMLs to become independent of interface density; in other words, the resistance at the interfaces becomes negligible, or the TBC increases beyond the ability to measure a quantifiable value. Supported with both vibrational spectroscopy and molecular dynamics simulations, we identify interfacial defect modes that arise in the thermal phonon regime only in the N_2-processed AMLs.

The amorphous SiOC:H/SiC:H multilayer samples were deposited on crystalline silicon substrates via plasma-enhanced chemical vapor deposition (PECVD). A sample series with N_2 plasma-treated multilayers, carried out in situ during growth between the deposition of either the SiOC:H or the SiC:H layers, were also fabricated to understand the effect of interfacial nonidealities that arise due to lighter atoms at the interface on mediating thermal transport across disordered interfaces. A schematic of the sample used for our thermal measurements is shown in **Figure 1**a. The film and period thicknesses were determined via X-ray reflectivity (XRR) and cross-section scanning electron microscopy (XSEM) measurements; example XSEM and XRR measurements are shown in Figure 1b,c, for a SiOC:H/SiC:H multilayer with N_2 plasma treatments carried out on the surface of the SiOC:H layers, and for a multilayer with N_2 plasma treatments carried out on the surface of the SiC:H layers, respectively. The chemical compositions of the multilayer films and homogeneous samples were determined using nuclear reaction analysis and Rutherford backscattering (RBS) spectroscopy (details in the Supporting Information). The percent composition of C, N, O, Si, and H is tabulated in Table S1 (Supporting Information). Along with the chemical compositions, the densities of the films were determined by combining the film compositions (in atoms cm^{-2}) with the measured film thicknesses and are tabulated in Table S1 (Supporting Information). The vibrational properties of the samples were studied using Fourier transform infrared (FTIR) spectroscopy. Figure 1d shows example spectra for different period thicknesses of SiOC:H/SiC:H multilayers with and without N_2 plasma. In comparison to the SiOC:H/SiC:H sample, the similarities between the FTIR spectra of the sample in which the SiC:H was treated with N_2 versus the sample in which the SiOC:H was treated with plasma suggests the N_2 plasma is enhancing the vibrations in the 20–30 THz range, as discussed in detail later.

To measure the thermal properties, we employed the time domain thermoreflectance (TDTR) technique, which is a noncontact optical pump-probe technique (details are given in the Supporting Information). First, we measure the thermal conductivity and heat capacity of individual SiOC:H and SiC:H films as a function of film thickness (as shown in Figure S7, Supporting Information). The lack of film thickness dependence on the thermal conductivity for the a-SiOC:H and a-SiC:H films suggests that heat conduction is mostly driven by vibrations that are nonpropagating (e.g., diffusons and locons).[18–20] This is in contrast to recent experimental results demonstrating size effects and anisotropic thermal conductivity of amorphous Si thin films and nanostructures,[21–23] where a significant portion of heat flow is due to propagons that represent delocalized propagating modes. The lack of size effects in the thermal conductivity of a-SiOC:H can be attributed to the Si—O—Si network structure confirmed from the FTIR measurements (Figure S3a, Supporting Information), which is similar to the structure found in SiO_2; the lack of size effects in SiO_2 is primarily due to the weak bonding that exists between the SiO_4 tetrahedra, whereas the thickness dependent thermal conductivity in a-Si is a result of strongly bonded tetrahedra.[18] Although cross-plane thermal conductivity measurements on thin amorphous SiO_2 films have revealed a lack of size effects,[21,23] we note that a recent study has observed ballistic propagation of thermal phonons across amorphous SiO_2 layers that are up to 5 nm thick. In this regard, although our SiOC:H and SiC:H films demonstrate lack of size effects in the cross plane direction, ballistic transport of phonons across thin layers of SiOC:H and SiC:H could be observed with the correct experimental techniques, such as that reported in ref. [24].

For the a-SiC:H films, the FTIR results show that the network structure mostly consists of Si—C stretching modes similar to a-SiC systems (as shown in Figure S3b, Supporting Information);[25,26] the lack of size effects in the a-SiC:H is consistent with size independent thermal conductivities measured for amorphous SiC in ref. [27]. These findings along with the measurement of heat capacities for the amorphous SiOC:H and SiC:H films and the measured thermal conductivities of amorphous SiOC:H/SiC:H SLs with varying period thicknesses are used to derive a mean TBC across a single SiOC:H/SiC:H interface as detailed in the discussions below.

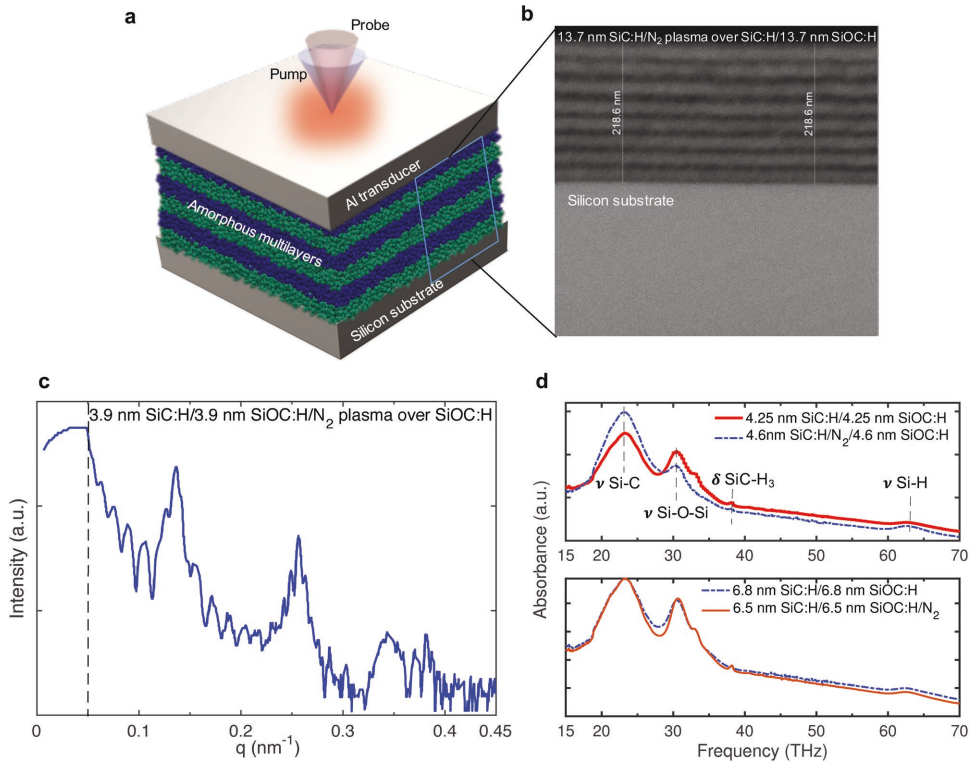

Figure 1. a) Schematic of a multilayer sample for our thermal measurements via the pump-probe TDTR technique. b) Characteristic XSEM image for a multilayer with 27.4 nm period thickness and N_2 plasma treatment carried out on the surface of SiC:H layers. The thickness and periodicity can be confirmed via the XSEM images. c) Characteristic XRR patterns showing superlattice reflections exemplified by the peaks in the XRR data for a (7.8 nm period thick) SiC:H/SiOC:H sample with N_2 plasma treatment over SiOC:H layers. d) Characteristic FTIR spectra for two representative samples with and without N_2 plasma treatment on the SiOC:H or SiC:H laminates in situ during growth.

The measured thermal conductivities of the amorphous SiOC:H/SiC:H superlattices are shown as a function of period lengths and interface densities in **Figure 2**a and 2b, respectively (square symbols). The thermal conductivity for SiC:H/SiOC:H SLs monotonically decreases with decreasing period thickness and increasing interface density. This suggests that the interfaces in the amorphous SLs contribute nonnegligibly to thermal resistance across the thin films. To determine the TBC across the SiC:H/SiOC:H interface, we apply the widely used thermal circuit model,[28] which describes the resistivity, ρ, of a SL as a superposition of the thermal resistances of the individual layers and the resistances at the individual interfaces as

$$\rho = \kappa^{-1} = \frac{1}{L}\left[\frac{L}{2\kappa_{\mathrm{SiOC:H}}} + \frac{L}{2\kappa_{\mathrm{SiC:H}}} + 2R_{\mathrm{K}}\right] \quad (1)$$

where $\kappa_{\mathrm{SiOC:H}}$ and $\kappa_{\mathrm{SiC:H}}$ are determined from the measurements of the thickness series for the respective homogeneous samples. Equation (1) is fit to the experimental data with R_{K} as the fitting parameter. Using this approach, we determine R_{K} = 1.1 m^2 K GW^{-1} (alternatively the TBC, $h_{\mathrm{K}} = 1/R_{\mathrm{K}}$ = 909 MW m^{-2} K^{-1}), resulting in the best-fit line shown in Figure 2.

This intrinsic TBC across our amorphous SiC:H/SiOC:H interfaces is considerably higher than mostly all TBCs reported in the literature for crystalline/crystalline interfaces as shown in **Figure 3**, which plots the experimentally measured TBCs across various interfaces as a function of the ratio of elastic moduli between the two constituents. Typical TBCs at crystalline/crystalline interfaces range from ≈20 to 300 MW m^{-2} K^{-1} and are shown in Figure 3 (in the shaded region in Figure 3). A better match between the elastic moduli of the crystalline materials forming the interface and a high quality of interface usually results in a higher TBC. For example, in ref. [40], it is shown that by controlling the surface condition between crystalline silicon nanomembranes mechanically joined on to silicon substrates through van der Waals interactions, the TBC can be tuned by as much as 300%. However, for interfaces comprising of amorphous solids, the measured TBCs can be relatively higher even for interfaces between materials with highly mismatched elastic moduli.

The high TBCs at these amorphous SiC:H/SiOC:H interfaces are in line with those predicted via molecular dynamics simulations (refs. [12] and [39]), experimentally measured across $SiO_2/Al2O_3$ interfaces reported from a single AML at room temperature (≈0.67 GW m^{-2} K^{-1}),[45] and the lower limit to TBC measured across an amorphous SiO_2/crystalline Si interface.[29] In ref. [39], we showed that the TBC across a generic Lennard Jones (LJ)-based amorphous/amorphous interface is higher than that of their crystalline counterpart, suggesting that TBC associated with amorphous interfaces are, in general, much higher than those across their corresponding crystalline interfaces. An analysis to predict the spectral contributions at the LJ-based amorphous/amorphous and crystalline/crystalline interfaces (as detailed in the Supporting Information)

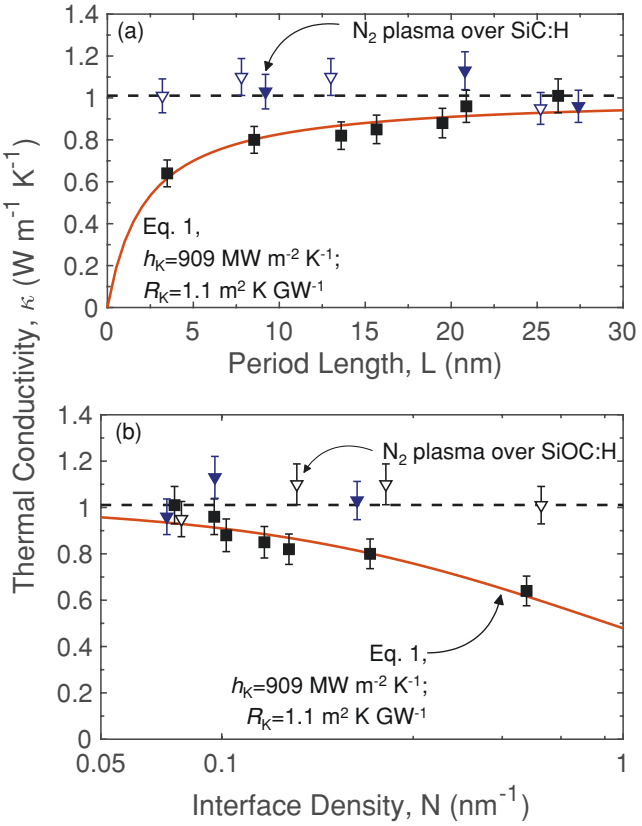

Figure 2. a,b) Thermal conductivities of amorphous SiOC:H/SiC:H superlattices plotted as a function of period length (a) and interface density (b). For comparison, thermal conductivities of N_2 plasma treated superlattices are also included. The solid square symbols represent AMLs without the N_2 plasma treatments. The hollow triangles represent AMLs with N_2 plasma treatment on the SiC:H layers, whereas the solid triangles represent AMLs with N_2 plasma treatment on the SiOC:H layers. The N_2 plasma is shown to increase the thermal conductivities of AMLs with smaller period thicknesses regardless of whether the plasma is applied on the SiC:H or SiOC:H layers.

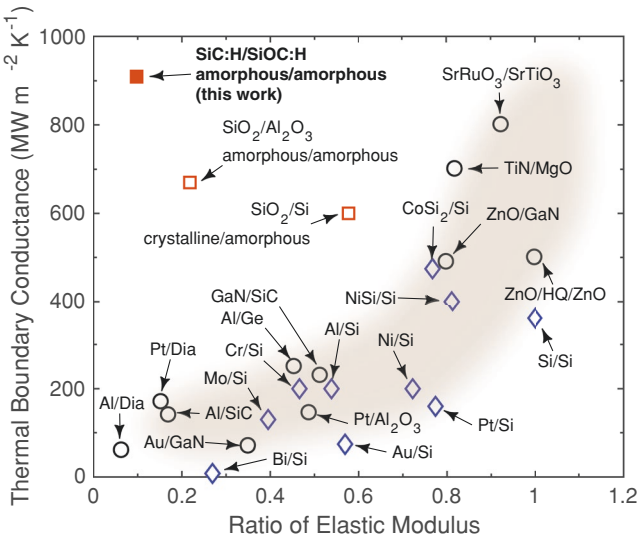

Figure 3. Experimentally measured thermal boundary conductance versus ratio of the elastic moduli of the two constituent materials (for Si/SiO_2,[29] Al/diamond, Pt/diamond,[30] Al/SiC,[31] Au/GaN,[32] Al/Ge,[33] GaN/SiC,[34] TiN/MgO,[35] $SrRuO_3/SrTiO_3$,[36] Pt/Al_2O_3,[37] ZnO/GaN,[38] ZnO/HQ/ZnO,[39] Si/vdW (van der Waals interface)/Si,[40] Bi/Si,[41] Mo/Si, Al/Si, Ni/Si,[42] Cr/Si, Pt/Si, Au/Si,[43] NiSi/Si, and $CoSi_2/Si$[44]).

suggests that vibrations carrying heat across interfaces are very different between the amorphous and crystalline phases. Along these lines, recent work has suggested that disorder around amorphous interfaces forces atomic vibrations near the interface to perturb the natural modes of vibrations in the amorphous materials, leading to higher frequency vibrations near the interface that effectively couple with one another.[12] Thus, in the event that the masses of these atoms are reduced, the local velocity that drives the cross-correlation of the heat flux will be increased. In this regard, the introduction of light atom impurities at amorphous interfaces should further increase the TBC by enabling a higher heat flux across the interface.

Figure 2 shows the thermal conductivity of the multilayers with N_2 plasma treatment carried out after either the SiOC:H or SiC:H layers are deposited. For both cases, when N_2 plasma is exposed on the SiOC:H layers or on the SiC:H layers, the thermal conductivity of the multilayers is independent of period thicknesses, in contrast to the results for the multilayers without the plasma treatment.

As shown in Table S1 (Supporting Information), the chemical compositions and the density of the multilayers do not change significantly due to the plasma treatment, which suggests that the varying thermal conductivity trends as shown in Figure 2 for our AMLs with/without plasma treatments is not due to densification or drastic changes in the composition and coordination number for these films. Furthermore, the thermal conductivity of samples with plasma treatment carried out at different thickness intervals for homogeneous SiC:H and SiOC:H films (i.e., SiC:H/N_2 plasma/SiC:H/N_2 plasma or SiOC:H/N_2 plasma/SiOC:H/N_2 plasma) do not change within uncertainty compared to the ones without the plasma treatment (Table S1, Supporting Information). These observations suggest that there is a different mechanism leading to an increase in the thermal conductivity of the N_2 plasma treated samples at high interface densities. To investigate this phenomenon further, we turn to material specific lattice dynamics calculations for our structures to assess how the vibrational modes change with N_2 plasma treatment. **Figure 4**a shows the density of states (DOS) for the interfacial modes predicted by a supercell lattice dynamics (SCLD) calculation for a short 2.5 nm period AML structure. The SCLD calculations used the ReaxFF potential to model the interatomic interactions[46] and the definition of an "interfacial mode" was taken to be the same as what was used previously by Gordiz and Henry.[11] Here, the interfacial region was taken to be all atoms within ±7 Å of the interface. As expected, since the two different systems contain different atom types in the interfacial region, the structures with and without nitrogen atoms at the interface exhibit differences in the interfacial modes that manifest. Most notably, there is a substantial increase (≈2 ×) in the total fraction of interfacial modes when the nitrogen is introduced. It should be noted that the total bulk DOS did not show a significant change overall when the computational domain contains N_2 atoms at the interfacial region, as is shown in Figure S8 (Supporting Information). There is, however, a significant change in the fraction of modes that are localized near the interface (increasing from 1.09 to 4.02% nitrogen atom concentration). This

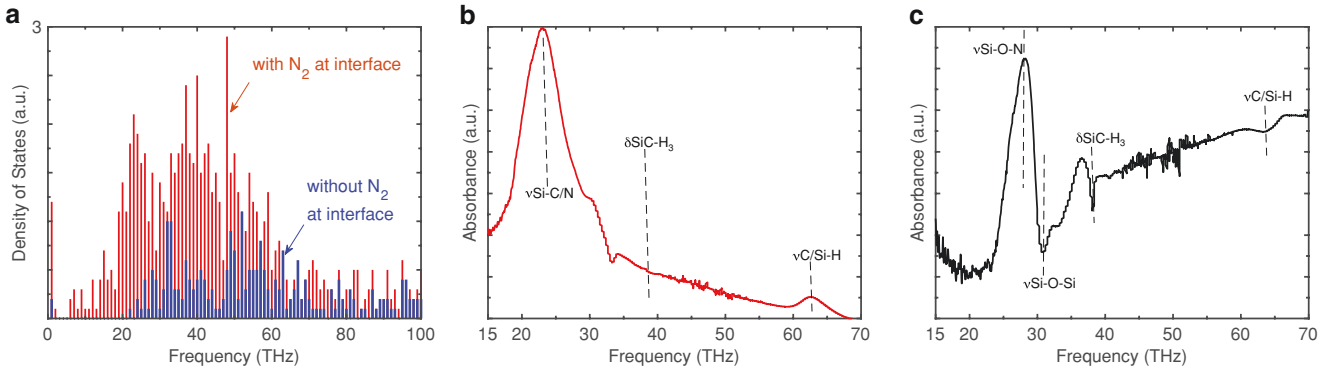

Figure 4. a) Calculated density of states for interfacial modes for the amorphous multilayers with and without N_2 atoms at the interface. The calculations were performed using supercell lattice dynamics (SCLD) and the interfacial mode definition was taken from prior work by Gordiz and Henry.[11] As expected, the presence of a different species of atoms in the interfacial region induces the formation of localized modes in that region. b,c) Subtracted FTIR spectra for SiC:H/SiOC:H multilayers with N_2 plasma treatment over SiC:H (b) and SiOC:H (c) with respect to a multilayer without the plasma treatment.

is to be expected, since new and uniquely tailored solutions to the equations of motion are required for the nitrogen atoms, which differ from the atoms everywhere else in the structure.

This is further validated by our FTIR measurements on the AMLs, shown in Figure 4b,c, where we plot the absorbance for the samples with the plasma treatment on the SiC:H and SiOC:H layers, respectively, which is subtracted from the absorbance for the multilayer with similar period thickness without the plasma treatments. There is some correspondence between the FTIR results and the changes in interfacial mode DOS. Notably, the most significant differences between the interfacial DOS in both cases arise in the 20–40 THz regime, where the highest FTIR absorption is observed. Furthermore, the subtracted FTIR results in Figure 4b,c show that the most significant differences occur in the same frequency interval 20–40 THz. For the multilayer with N_2 exposed to the SiC:H layers, there is a clear increase in the vibrational bands at ≈24 THz that are associated with Si—C and Si—N bonds. For the case where we ran the N_2 plasma on top of the SiOC:H, we clearly see the appearance of an Si—O/N mode at ≈27 THz. This corresponds with a decrease in absorbance for the Si—O—Si stretching mode, SiC—H_3 deformation mode, and C—H stretching mode as shown by the dips in the absorbance spectra in Figure 4c. Taken together, the FTIR results are consistent with our SCLD-calculated DOS increase for these modes, which arise at the interface. Given that the total DOS for both structures is virtually indistinguishable (as shown in Figure S9, Supporting Information), and the fact that there is a noticeable change in the FTIR results suggests that the interfacial modes, which are different for the two structures, may be responsible for the difference in IR absorption.

To rule out the possibility that the increase in thermal conductivity of the N_2 plasma treated AMLs is solely due to the increase in their elastic modulus, we perform nonindentation measurements on all the samples (results are listed in Table S1, Supporting Information). The increase in interface density leads to a monotonically increasing elastic moduli. Moreover, the AMLs with the largest period thicknesses demonstrate similar elastic moduli as that for the softer SiOC:H sample. However, as the period thicknesses decrease, the modulus approaches a value that is similar to the average of the elastic moduli for SiC:H and SiOC:H. In terms of the measured thermal conductivities, even though the samples with N_2 plasma treatment show similar monotonic increase in elastic modulus as that for the nontreated samples, the thermal conductivity trends with interface density are different. This suggests that the increase in modulus for the N_2 plasma treated samples cannot explain the differing thermal conductivity trends between the N_2 plasma treated and nontreated samples as shown in Figure 2.

From these discussions and observations, we can attribute the increase in thermal conductivity and subsequent negligible interfacial resistance for the plasma-treated samples, as shown in Figure 2, to the incorporation of defect vibrational modes at the interfacial region that enhance the heat transport across the interfaces in our AMLs. These results suggest that the TBC at these already ultrahigh TBC interfaces can increase to values >1 GW m^{-2} K^{-1} with the inclusion of nitrogen interfacial defects and subsequent emergence of high-frequency interfacial vibrational modes. Our results demonstrate a path toward engineering TBC, thus providing a novel approach to dissipate the ever-increasing amounts of waste heat in microelectronic devices and alleviate the concern for the continuation of Moore's law. This work provides experimental and computational frameworks guiding future research on the manipulation of interfacial heat flow via inclusion of defect atoms with varying masses and bonding environments at the interfaces.

Supporting Information

Supporting Information is available from the Wiley Online Library or from the author.

Acknowledgements

This work was supported in part by the Office of Naval research, Grant. No. N00014-15-12769 and under a MURI program, Grant No. N00014-18-1-2429. This work was also supported in part by NSF Career Award No. 1554050.

Conflict of Interest

The authors declare no conflict of interest.

Keywords

amorphous multilayers, thermal boundary conductance, thermal conductivity

Received: June 27, 2018
Revised: August 2, 2018
Published online: September 17, 2018

[1] C. Chiritescu, D. G. Cahill, N. Nguyen, D. Johnson, A. Bodapati, P. Keblinski, P. Zschack, *Science* **2007**, *315*, 351.
[2] R. M. Costescu, D. G. Cahill, F. H. Fabreguette, Z. A. Sechrist, S. M. George, *Science* **2004**, *303*, 989.
[3] G. Pernot, M. Stoffel, I. Savic, F. Pezzoli, P. Chen, G. Savelli, A. Jacquot, J. Schumann, U. Denker, I. Mönch, C. Deneke, O. G. Schmidt, J. M. Rampnoux, S. Wang, M. Plissonnier, A. Rastelli, S. Dilhaire, N. Mingo, *Nat. Mater.* **2010**, *9*, 491.
[4] M. D. Losego, I. P. Blitz, R. A. Vaia, D. G. Cahill, P. V. Braun, *Nano Lett.* **2013**, *13*, 2215.
[5] E. Dechaumphai, D. Lu, J. J. Kan, J. Moon, E. E. Fullerton, Z. Liu, R. Chen, *Nano Lett.* **2014**, *14*, 2448.
[6] A. Einstein, *Ann. Phys.* **1911**, *340*, 679.
[7] K. Sääskilahti, J. Oksanen, J. Tulkki, S. Volz, *Phys. Rev. B* **2014**, *90*, 134312.
[8] Y. Chalopin, S. Volz, *Appl. Phys. Lett.* **2013**, *103*, 051602.
[9] J. C. Duda, T. S. English, E. S. Piekos, W. A. Soffa, L. V. Zhigilei, P. E. Hopkins, *Phys. Rev. B* **2011**, *84*, 193301.
[10] T. Murakami, T. Hori, T. Shiga, J. Shiomi, *Appl. Phys. Express* **2014**, *7*, 121801.
[11] K. Gordiz, A. Henry, *J. Appl. Phys.* **2016**, *119*, 015101.
[12] K. Gordiz, A. Henry, *J. Appl. Phys.* **2017**, *121*, 025102.
[13] A. Giri, P. E. Hopkins, J. G. Wessel, J. C. Duda, *J. Appl. Phys.* **2015**, *118*, 165303.
[14] E. T. Swartz, R. O. Pohl, *Rev. Mod. Phys.* **1989**, *61*, 605.
[15] P. Reddy, K. Castelino, A. Majumdar, *Appl. Phys. Lett.* **2005**, *87*, 211908.
[16] R. Prasher, *Appl. Phys. Lett.* **2009**, *94*, 041905.
[17] A. Grill, S. M. Gates, T. E. Ryan, S. V. Nguyen, D. Priyadarshini, *Appl. Phys. Rev.* **2014**, *1*, 011306.
[18] J. M. Larkin, A. J. H. McGaughey, *Phys. Rev. B* **2014**, *89*, 144303.
[19] P. B. Allen, J. L. Feldman, *Phys. Rev. B* **1993**, *48*, 12581.
[20] P. B. Allen, J. L. Feldman, J. Fabian, F. Wooten, *Philos. Mag. B* **1999**, *79*, 1715.
[21] J. L. Braun, C. H. Baker, A. Giri, M. Elahi, K. Artyushkova, T. E. Beechem, P. M. Norris, Z. C. Leseman, J. T. Gaskins, P. E. Hopkins, *Phys. Rev. B* **2016**, *93*, 140201.
[22] S. Kwon, J. Zheng, M. C. Wingert, S. Cui, R. Chen, *ACS Nano* **2017**, *11*, 2470.
[23] M. C. Wingert, J. Zheng, S. Kwon, R. Chen, *Semicond. Sci. Technol.* **2016**, *31*, 113003.
[24] L. Yang, Q. Zhang, Z. Cui, M. Gerboth, Y. Zhao, T. T. Xu, D. G. Walker, D. Li, *Nano Lett.* **2017**, *17*, 7218.
[25] J. Chen, S. W. King, E. Muthuswamy, A. Koryttseva, D. Wu, A. Navrotsky, *J. Am. Ceram. Soc.* **2016**, *99*, 2752.
[26] S. King, M. French, J. Bielefeld, W. Lanford, *J. Non-Cryst. Solids* **2011**, *357*, 2970.
[27] T. Jeong, J.-G. Zhu, S. Mao, T. Pan, Y. J. Tang, *Int. J. Thermophys.* **2012**, *33*, 1000.
[28] Y. K. Koh, Y. Cao, D. G. Cahill, D. Jena, *Adv. Funct. Mater.* **2009**, *19*, 610.
[29] J. Kimling, A. Philippi-Kobs, J. Jacobsohn, H. P. Oepen, D. G. Cahill, *Phys. Rev. B* **2017**, *95*, 184305.
[30] G. T. Hohensee, R. B. Wilson, D. G. Cahill, *Nat. Commun.* **2015**, *6*, 6578.
[31] X. Qian, P. Jiang, R. Yang, *Mater. Today Phys.* **2017**, *3*, 70.
[32] B. F. Donovan, C. J. Szwejkowski, J. C. Duda, R. Cheaito, J. T. Gaskins, C.-Y. P. Yang, C. Constantin, R. E. Jones, P. E. Hopkins, *Appl. Phys. Lett.* **2014**, *105*, 203502.
[33] R. B. Wilson, D. G. Cahill, *Nat. Commun.* **2014**, *5*, 5075.
[34] E. Ziade, J. Yang, G. Brummer, D. Nothern, T. Moustakas, A. J. Schmidt, *Appl. Phys. Lett.* **2015**, *107*, 091605.
[35] R. M. Costescu, M. A. Wall, D. G. Cahill, *Phys. Rev. B* **2003**, *67*, 054302.
[36] R. B. Wilson, B. A. Apgar, W. P. Hsieh, L. W. Martin, D. G. Cahill, *Phys. Rev. B* **2015**, *91*, 115414.
[37] P. E. Hopkins, R. J. Stevens, P. M. Norris, *J. Heat Transfer* **2008**, *130*, 022401.
[38] J. T. Gaskins, G. Kotsonis, A. Giri, C. T. Shelton, E. Sachet, Z. Cheng, B. M. Foley, Z. Liu, S. Ju, J. Shiomi, M. S. Goorsky, S. Graham, T. Luo, A. Henry, J. P. Maria, P. E. Hopkins, ArXiv e-prints **2017**, arXiv:1710.09525 [cond-mat.mtrl-sci].
[39] A. Giri, J. P. Niemelä, T. Tynell, J. T. Gaskins, B. F. Donovan, M. Karppinen, P. E. Hopkins, *Phys. Rev. B* **2016**, *93*, 115310.
[40] D. P. Schroeder, Z. Aksamija, A. Rath, P. M. Voyles, M. G. Lagally, M. A. Eriksson, *Phys. Rev. Lett.* **2015**, *115*, 256101.
[41] R. J. Stoner, H. J. Maris, T. R. Anthony, W. F. Banholzer, *Phys. Rev. Lett.* **1992**, *68*, 1563.
[42] R. Cheaito, J. T. Gaskins, M. E. Caplan, B. F. Donovan, B. M. Foley, A. Giri, J. C. Duda, C. J. Szwejkowski, C. Constantin, H. J. Brown-Shaklee, J. F. Ihlefeld, P. E. Hopkins, *Phys. Rev. B* **2015**, *91*, 035432.
[43] R. J. Stevens, A. N. Smith, P. M. Norris, *J. Heat Transfer* **2005**, *127*, 315.
[44] N. Ye, J. P. Feser, S. Sadasivam, T. S. Fisher, T. Wang, C. Ni, A. Janotti, *Phys. Rev. B* **2017**, *95*, 085430.
[45] S. W. Fong, A. Sood, L. Chen, N. Kumari, M. Asheghi, K. E. Goodson, G. A. Gibson, H. S. P. Wong, *J. Appl. Phys.* **2016**, *120*, 015103.
[46] A. C. T. van Duin, S. Dasgupta, F. Lorant, W. A. Goddard, *J. Phys. Chem. A* **2001**, *105*, 9396.

